UMN–TH–1811/99
TPI–MINN–99/36
MADPH-99-1125
hep-ph/9908311
August 1999

Variations of the Neutralino Elastic Cross-Section with CP Violating Phases

Toby Falk

Department of Physics, University of Wisconsin, Madison, WI 53706, USA

Andrew Ferstl and Keith A. Olive

Theoretical Physics Institute, School of Physics and Astronomy,
University of Minnesota, Minneapolis, MN 55455, USA

Abstract

We analyze the neutralino-nucleus elastic cross-section in the MSSM, including contributions from CP-violating phases, using the four-fermi neutralino-quark interaction. Over a wide range of the MSSM parameter space we show the variations in the cross-sections due to these phases. We further concentrate on the regions which are consistent with constraints from the electric dipole moment of the electron, neutron and mercury atom. In the regions we examine in detail, we find suppressions by up to a factor of two, while enhancements in the cross-sections are no greater than $\sim 10\%$.

1 Introduction

Supersymmetry provides a framework for constructing new models for physics beyond the standard model. The motivations for supersymmetry are well known, and include a stabilization of the mass hierarchy problem and unification of gauge couplings at the GUT scale. In the minimal supersymmetric extension of the standard model (MSSM) [1], conservation of R-parity, which can be related to baryon number, lepton number and spin, guarantees that the lightest supersymmetric partner (LSP) is stable and provides a candidate for the non-baryonic dark matter in the universe. Neutralinos, mixtures of neutral gauginos and Higgsinos, are the best motivated LSP candidate in the MSSM [2].

For a given set of MSSM parameters, the exact identity of the LSP is determined, its annihilation cross-section and hence its relic density can be calculated, as can its interactions with ordinary matter. The latter is key in efforts to detect MSSM dark matter in laboratory experiments [3, 4]. Indeed, over the years a great effort has been made to study the elastic cross-section of the LSP with nuclei in order to predict the possible detection rates in cryogenic detectors. Recently, it has been shown [5, 6, 7] that the CP violating phases in the MSSM may have significant effects on the detection rate of the neutralino. Here we continue our investigation of the neutralino-nucleon elastic cross-section over a wide range of MSSM parameters and show that these phases can give significant, variations to the cross-section. We also take into account the experimental electric dipole constraints of the electron, neutron and mercury atom, and show that variations in the cross-sections of order 0.4 – 1.1 persist.

CP violating phases can arise from several sources in the MSSM: the Higgs mixing mass (μ) in the superpotential, and the supersymmetry breaking parameters which includes the gaugino masses (M_i), the soft scalar masses, the bilinear term ($B\mu$), and the trilinear terms (A_f). Not all of these phases are physical [8]. For our purposes, the phases associated with the gaugino masses are rotated away and $B\mu$ will be taken as real so that the vacuum expectation values of the Higgs fields are real. Also, the phases of the trilinear terms, A_f (with the exception of A_t), will be set equal to one another, for simplicity. The trilinear stop mixing parameter A_t has a (real) quasi-fixed point in its evolution from the GUT scale to the electroweak scale, so we take A_t real. Then, the only physical phases in the MSSM are the phase associated with μ (θ_μ) and the phase associated with the A_f (θ_A). Typically, in order to satisfy constraints[9] on the electric dipole moment (EDM) of the electron, neutron and ^{199}Hg atom, CP violating phases must take on very small values (on the order of $10^{-2} - 10^{-3}$ for MSSM parameters on the order of 100 GeV). This limit can be weakened [10, 11] if the

SUSY masses are taken to be upwards of a TeV, which is not a cosmological viability if the neutralino is gaugino-like[12]. Models with heavy first two generations of sfermions and a light third generation[13], on the other hand, may allow large phases while permitting the neutralino to annihilate into e.g. tau pairs, so that the cosmological constraints are satisfied. Alternatively, with two CP violating phases and several contributions to the electric dipole moments cancellations can occur and allow the CP violating phases to take on larger values [14] - [18]. We neglect the (typically small) phase misalignment between the Higgs vevs, which is induced by one loop corrections to the Higgs potential in the presence of CP violation in the stop sector [19, 20]. The effect of this misalignment may be significant for large $|\mu A_t|/m_A^2$, particularly at large $\tan\beta$.

Previous studies [5, 6] have shown that the CP-violating phases can have a large effect on neutralino-nucleus elastic scattering cross-sections. In certain regions of the parameter space, the elastic cross-section with matter can show a dramatic dependence (usually a minimum) as a function of the CP violating phase θ_μ. Here, this effect is studied in more detail. In particular, we determine the dependence of the cross-section on the phases across the M_2-μ plane in the MSSM, including a separate investigation of the phase dependence of the spin-dependent and spin-independent cross-sections. We also examine the effect of the constraints of the electric dipole moments on the variation of the cross-section with respect to the phases. Generically, the EDM constraints require the phases to be sufficiently small that the cross-sections are only very mildly affected. Nevertheless, we do find parameter regions, predominantly where the neutralino is gaugino(bino)-like, where the constraints on the CP violating phases can be satisfied, and where the phases still produce significant changes to the scattering cross-section. In these regions, we find that the elastic cross-section may be enhanced by $\sim 10\%$ or reduced by as much as a factor of 2.5.

In Section 2, the effective neutralino-quark interaction Lagrangian is presented and the dominant terms in the direct detection rate are discussed. In Section 3, the analytic expression for the neutralino-nucleus scattering cross-section is found using the low energy effective Lagrangian. Finally, in Section 4 the variation of the elastic cross-section with the CP violating phases is shown. First, the effect of the phases on the spin-dependent, spin-independent, and total scattering rates is displayed for a particular set of parameters on the $M_2 - \mu$ plane. For these plots, no EDM constraints are imposed so that the general behavior with respect to the CP violating phases can be shown. Then a general scan of parameter space is performed while imposing the electron, neutron and mercury EDM constraints so that a consistent and realistic understanding of the effect of CP-violation can be shown.

2 Effective Lagrangian

The neutralino LSP is the lowest mass eigenstate of the linear combination of the bino, wino, and Higgsinos. In our notation,

$$\chi = Z_{\chi 1}\tilde{B} + Z_{\chi 2}\tilde{W} + Z_{\chi 3}\tilde{H}_1 + Z_{\chi 4}\tilde{H}_2 \tag{1}$$

The neutralino mass matrix in the $(\tilde{B}, \tilde{W}, \tilde{H}_1, \tilde{H}_2)$ basis is:

$$N = \begin{pmatrix} M_1 & 0 & -M_Z \sin\theta_W \cos\beta & M_Z \sin\theta_W \sin\beta \\ 0 & M_2 & M_Z \cos\theta_W \cos\beta & -M_Z \cos\theta_W \sin\beta \\ -M_Z \sin\theta_W \cos\beta & M_Z \cos\theta_W \cos\beta & 0 & -\mu \\ M_Z \sin\theta_W \sin\beta & -M_Z \cos\theta_W \sin\beta & -\mu & 0 \end{pmatrix},$$

where M_1 and M_2 are the U(1) and SU(2) gaugino masses, $\tan\beta$ is the ratio of the Higgs vacuum expectation values, and μ is the Higgsino mixing mass. We assume a common gaugino mass at the GUT scale, which gives $M_1 = \frac{5}{3}\tan^2\theta_W M_2$, and we take $\tan\beta, \mu$, and M_2 as free parameters. The mass matrix is diagonalized by a matrix Z, $Z^* N Z^{-1}$, which determines the eigenstate composition in (1).

The sfermion mass^2 matrix can be written as

$$M^2 = \begin{pmatrix} M_L^2 + m_f^2 + \cos 2\beta (T_{3f} - Q_f \sin^2\theta_W) M_Z^2 & -m_f \overline{m}_f e^{i\gamma_f} \\ -m_f \overline{m}_f e^{-i\gamma_f} & M_R^2 + m_f^2 + Q_f \sin^2\theta_W M_Z^2 \cos 2\beta \end{pmatrix}.$$

Here, $M_{L(R)}$ are the soft supersymmetry breaking sfermion masses which are real since we have assumed that they are generation independent and generation diagonal. Also,

$$\overline{m}_f e^{i\gamma_f} = R_f \mu + A_f^* = R_f \left|\mu\right| e^{i\theta_\mu} + \left|A_f\right| e^{-i\theta_A} \tag{2}$$

where m_f is the mass of the fermion and $R_f = \cot\beta(\tan\beta)$ for weak isospin +1/2 (-1/2) fermions. For simplicity, we will choose all A_f, except for A_t, to be degenerate at the weak scale, in our analysis. When the top quark Yukawa coupling is large at the GUT scale, the initial value of A_t at M_{GUT} tends to be damped as A_t is evolved, and $m_{1/2}$ sets the scale of A_t at the weak scale. A_t is therefore set equal to its quasi-fixed point value $\approx 2m_{1/2}$ [21]. Here $m_{1/2}$ is the common gaugino mass at the GUT scale and is equal to $4M_2\pi\alpha_{GUT}/g^2$, where we've taken $1/\alpha_{GUT} = 24.85$. Finally, the sfermion mass^2 matrix is diagonalized by a matrix η, $\eta M^2 \eta^{-1}$, and can be parameterized by an angle θ_f with

$$\begin{pmatrix} \cos\theta_f & \sin\theta_f e^{i\gamma_f} \\ -\sin\theta_f e^{-i\gamma_f} & \cos\theta_f \end{pmatrix} \equiv \begin{pmatrix} \eta_{11} & \eta_{12} \\ \eta_{21} & \eta_{22} \end{pmatrix}$$

From the MSSM Lagrangian, we deduce the low energy effective four-fermi Lagrangian:

$$L = \bar{\chi}\gamma^{\mu}\gamma^{5}\chi\bar{q}_i\gamma_{\mu}(\alpha_{1i} + \alpha_{2i}\gamma^{5})q_i + \alpha_{3i}\bar{\chi}\chi\bar{q}_i q_i + \alpha_{4i}\bar{\chi}\gamma^{5}\chi\bar{q}_i\gamma^{5}q_i + \alpha_{5i}\bar{\chi}\chi\bar{q}_i\gamma^{5}q_i + \alpha_{6i}\bar{\chi}\gamma^{5}\chi\bar{q}_i q_i \quad (3)$$

The Lagrangian is to be summed over the quark generations, and the subscript i refers to up-type quarks (i=1) and down-type quarks (i=2). The coefficients α are:

$$\begin{aligned}
\alpha_{1i} &= -\frac{1}{4(m_{1i}^2 - m_{\chi}^2)}\left[|Y_i|^2 - |X_i|^2\right] - \frac{1}{4(m_{2i}^2 - m_{\chi}^2)}\left[|V_i|^2 - |W_i|^2\right] \\
&\quad + \frac{g^2}{4m_z^2\cos^2\theta_w}\left[|Z_{\chi_3}|^2 - |Z_{\chi_4}|^2\right]\frac{T_{3i} - 2e_i\sin^2\theta_w}{2} \qquad (4)
\end{aligned}$$

$$\begin{aligned}
\alpha_{2i} &= \frac{1}{4(m_{1i}^2 - m_{\chi}^2)}\left[|Y_i|^2 + |X_i|^2\right] + \frac{1}{4(m_{2i}^2 - m_{\chi}^2)}\left[|V_i|^2 + |W_i|^2\right] \\
&\quad - \frac{g^2}{4m_z^2\cos^2\theta_w}\left[|Z_{\chi_3}|^2 - |Z_{\chi_4}|^2\right]\frac{T_{3i}}{2} \qquad (5)
\end{aligned}$$

$$\begin{aligned}
\alpha_{3i} &= -\frac{1}{2(m_{1i}^2 - m_{\chi}^2)}Re\left[(X_i)(Y_i)^*\right] - \frac{1}{2(m_{2i}^2 - m_{\chi}^2)}Re\left[(W_i)(V_i)^*\right] \\
&\quad - \frac{gm_{qi}}{4m_w B_i}\left[Re\left(\delta_{1i}[gZ_{\chi 2} - g'Z_{\chi 1}]\right)D_i C_i\left(-\frac{1}{m_{H_1}^2} + \frac{1}{m_{H_2}^2}\right)\right. \\
&\quad \left. + Re\left(\delta_{2i}[gZ_{\chi 2} - g'Z_{\chi 1}]\right)\left(\frac{D_i^2}{m_{H_2}^2} + \frac{C_i^2}{m_{H_1}^2}\right)\right] \qquad (6)
\end{aligned}$$

$$\begin{aligned}
\alpha_{4i} &= -\frac{1}{2(m_{1i}^2 - m_{\chi}^2)}Re\left[(X_i)(Y_i)^*\right] - \frac{1}{2(m_{2i}^2 - m_{\chi}^2)}Re\left[(W_i)(V_i)^*\right] \\
&\quad - \frac{gm_{qi}A_i}{4m_w B_i m_{H_3}^2}\left[-B_i Re\left(\delta_{1i}[gZ_{\chi 2} - g'Z_{\chi 1}]\right)\right. \\
&\quad \left. + A_i Re\left(\delta_{2i}[gZ_{\chi 2} - g'Z_{\chi 1}]\right)\right] \qquad (7)
\end{aligned}$$

$$\begin{aligned}
\alpha_{5i} &= -\frac{i}{2(m_{1i}^2 - m_{\chi}^2)}Im\left[(Y_i)(X_i)^*\right] - \frac{i}{2(m_{2i}^2 - m_{\chi}^2)}Im\left[(V_i)(W_i)^*\right] \\
&\quad + \frac{igm_{qi}A_i}{4m_{H_3}^2 m_w B_i}\left[B_i Im\left(\delta_{1i}[gZ_{\chi 2} - g'Z_{\chi 1}]\right)\right. \\
&\quad \left. - A_i Im\left(\delta_{2i}[gZ_{\chi 2} - g'Z_{\chi 1}]\right)\right] \qquad (8)
\end{aligned}$$

$$\begin{aligned}\alpha_{6i} &= -\frac{i}{2(m_{1i}^2-m_\chi^2)}Im\left[(Y_i)\,(X_i)^*\right]-\frac{i}{2(m_{2i}^2-m_\chi^2)}Im\left[(V_i)\,(W_i)^*\right]\\ &-\frac{igm_{qi}}{4m_wB_i}\left[Im\left(\delta_{1i}[gZ_{\chi 2}-g'Z_{\chi 1}]\right)D_iC_i\left(-\frac{1}{m_{H_1}^2}+\frac{1}{m_{H_2}^2}\right)\right.\\ &\left.+Im\left(\delta_{2i}[gZ_{\chi 2}-g'Z_{\chi 1}]\right)\left(\frac{D_i^2}{m_{H_2}^2}+\frac{C_i^2}{m_{H_1}^2}\right)\right] \qquad (9)\end{aligned}$$

Where

$$\begin{aligned}X_i &= \eta_{11}^*\frac{gm_{q_i}Z_{\chi 5-i}^*}{2m_wB_i}-\eta_{12}^*e_ig'Z_{\chi 1}^*\\ Y_i &= \eta_{11}^*\left(\frac{y_i}{2}g'Z_{\chi 1}+gT_{3i}Z_{\chi 2}\right)+\eta_{12}^*\frac{gm_{q_i}Z_{\chi 5-i}}{2m_wB_i}\\ W_i &= \eta_{21}^*\frac{gm_{q_i}Z_{\chi 5-i}^*}{2m_wB_i}-\eta_{22}^*e_ig'Z_{\chi 1}^*\\ V_i &= \eta_{22}^*\frac{gm_{q_i}Z_{\chi 5-i}}{2m_wB_i}+\eta_{21}^*\left(\frac{y_i}{2}g'Z_{\chi 1}+gT_{3i}Z_{\chi 2}\right) \qquad (10)\end{aligned}$$

Here, δ_{1i} is $Z_{\chi 3}$ ($Z_{\chi 4}$), δ_{2i} is $Z_{\chi 4}$ ($-Z_{\chi 3}$), B_i is $\sin\beta$ ($\cos\beta$), A_i is $\cos\beta$ ($-\sin\beta$), C_i is $\sin\alpha$ ($\cos\alpha$), and D_i is $\cos\alpha$ ($-\sin\alpha$) for up (down) type quarks. The masses, m_1 and m_2 correspond to the two squark mass eigenstates. $m_{H_{1,2,3}}$ are the two scalar and pseudoscalar Higgs masses respectively (H_2 is the lighter scalar). α is the Higgs mixing angle. We note that (6) corrects an error in [5], where the expressions for α_2 and α_3 were presented previously. y_i is the hypercharge defined by $e_i = T_{3i} + y_i/2$. The expressions for the α_i agree with those in [6].[1] Also, in the limit of vanishing CP-violating phases, the spin-independent term, proportional to α_{3i}, and the spin-dependent term, proportional to α_{2i}, agree with those in [4] and [22].

From the Lagrangian we can calculate the cross-section of a neutralino scattering off of a target nucleus. All the terms in the Lagrangian, however, do not contribute equally to the cross-section. For example,

$$|\langle f|\alpha_{4i}\bar{\chi}\gamma_5\chi\bar{q}_i\gamma_5q_i|i\rangle|^2 \propto |\zeta_{5i}|^2||\alpha_{4i}|^2\frac{(-p_{\chi_f}\cdot p_{\chi_i}+m_\chi^2)}{m_\chi^2}\frac{(-p_{N_f}\cdot p_{N_i}+m_N^2)}{m_N^2} \qquad (11)$$

$$|\langle f|\alpha_{5i}\bar{\chi}\chi\bar{q}_i\gamma_5q_i|i\rangle|^2 \propto |\zeta_{5i}|^2||\alpha_{5i}|^2\frac{(-p_{N_f}\cdot p_{N_i}+m_N^2)}{m_N^2} \qquad (12)$$

[1] Our expressions agree with the corrected expressions in a revised version of [6] as communicated to us by the authors.

$$\left|\langle f|\alpha_{6i}\bar{\chi}\gamma^5\chi\bar{q}_i q_i|i\rangle\right|^2 \propto |\zeta_i|^2|\alpha_{6i}|^2\frac{(-p_{\chi_f}\cdot p_{\chi_i}+m_\chi^2)}{m_\chi^2} \tag{13}$$

where the p_i are the four-momenta of the particle i. In the non-relativistic limit, the expressions (11)-(13) have a leading term proportional to the three momentum of the neutralino squared, the three momentum of the nucleus squared, or both. Here, $\zeta_i = \langle N|\bar{q}_i q_i|N\rangle$, and $\zeta_{5i} = \langle N|\bar{q}_i\gamma_5 q_i|N\rangle$, which corresponds to the quark contribution to the nucleon spin and is discussed in detail in [23]. The axial-vector term represented by α_{1i} is also found to be negligible [24]

$$\begin{aligned}&|\langle f|\alpha_{1i}\bar{\chi}\gamma_\mu\gamma_5\chi\bar{q}_i\gamma_\mu q_i|i\rangle|^2 \propto \\ &\quad|\alpha_{1i}|^2\frac{p_{\chi_f}p_{N_f}(p_{\chi_i}p_{N_i})+p_{\chi_f}p_{N_i}(p_{\chi_i}p_{N_f})+p_{N_f}p_{N_i}m_\chi^2-p_{\chi_f}p_{\chi_i}m_N^2-2m_\chi^2m_N^2}{m_\chi^2m_N^2}\end{aligned} \tag{14}$$

In the non-relativistic limit, this reduces to a combination of the three momentum squared of the neutralino and nucleus. These terms are, hence, negligible compared to the terms multiplied by α_{2i} and α_{3i} which are not directly proportional to any three-momenta in the non-relativistic limit [25].

The expressions for α_{2i} and α_{3i} in equations (5) and (6) therefore, dominate the elastic cross-section. These expressions receive contributions arising from squark, Z^o, and both scalar Higgs boson exchanges. The term proportional to α_{2i} (equation (5)) is a spin dependent coupling of the LSP to the nucleus due to the $\gamma_\mu\gamma_5$ factor, which is the spin projection in the non relativistic limit [24]. On the other hand, the term proportional to α_{3i} (equation (6)) results in a coherent scattering of the LSP with the nucleus and as such is proportional to the mass of the nucleus. For large A nuclei, this term may be large for much of the MSSM parameter space. The steps to finding the cross-section from the effective Lagrangian are laid out in [4] and outlined below.

3 Evaluating the Cross-Section

The spin dependent cross-section can be written as

$$\sigma_2 = \frac{32}{\pi}G_f^2 m_r^2\Lambda^2 J(J+1) \tag{15}$$

where m_r is the reduced neutralino-nucleus mass, J is the spin of the nucleus and

$$\Lambda = \frac{1}{J}(a_p\langle S_p\rangle + a_n\langle S_n\rangle) \tag{16}$$

where

$$a_p = \sum_i \frac{\alpha_{2i}}{\sqrt{2}G_f}\Delta_i^{(p)}, a_n = \sum_i \frac{\alpha_{2i}}{\sqrt{2}G_f}\Delta_i^{(n)} \tag{17}$$

The factors $\Delta_i^{(p,n)}$ depend on the spin content of the nucleon and are taken here to be $\Delta_i^{(p)} = 0.77, -0.38, -0.09$ for u, d, s respectively and $\Delta_u^{(n)} = \Delta_d^{(p)}, \Delta_d^{(n)} = \Delta_u^{(p)}, \Delta_s^{(n)} = \Delta_s^{(p)}$ [26] The expectation values of the spin content of the nucleus, $\langle S_{p,n}\rangle$, depend on the target nucleus. Our results are for ^{73}Ge, which has $\langle S_{p,n}\rangle = 0.011, 0.491$, and for ^{19}F, which has $\langle S_{p,n}\rangle = 0.415, -0.047$. The reader may refer to [4] for details on these quantities.

The spin-independent cross-section can be written as

$$\sigma_3 = \frac{4m_r^2}{\pi}\left[Zf_p + (A-Z)f_n\right]^2 \tag{18}$$

where

$$\frac{f_p}{m_p} = \sum_{q=u,d,s} f_{Tq}^{(p)}\frac{\alpha_{3q}}{m_q} + \frac{2}{27}f_{TG}^{(p)}\sum_{c,b,t}\frac{\alpha_{3q}}{m_q} \tag{19}$$

and f_n has a similar expression. The parameters $f_{Tq}^{(p)}$ are defined by $\langle p|m_q\bar{q}q|p\rangle = m_p f_{Tq}^{(p)}$, while $f_{TG}^{(p)} = 1 - \sum_{q=u,d,s} f_{Tq}^{(p)}$ [27]. Our results used $f_{Tq}^{(p)} = 0.019, 0.041, 0.14$ for u, d, s and $f_{Tq}^{(n)} = 0.023, 0.034, 0.14$ [28]. There are other contributions to the spin-independent cross-section that depend on loop effects for heavy quarks and twist-2 operators which have been shown to be numerically small [29] and are not included here. Note from (6) and (10) that the spin-independent cross-section is suppressed by the small nucleon mass. However, in contrast to the spin-dependent cross-section, the spin-independent cross-section scales with the atomic weight of the scattering nucleus and therefore can dominate for heavy nuclei. We show results for ^{73}Ge, which has predominantly spin-independent interactions, and ^{19}F, for which either interaction can dominate, depending on the parameter region.

The CP-violating phases can impact the cross-section in several ways. The phases can change the mass of the LSP. They will also change $Z_{\chi i}$, which indicate the identity of the LSP, as well as the η_{ij}, which indicate the mass eigenstates (and eigenvalues) of the sfermions. To get an understanding of how these effects arise, consider the case of the LSP being a nearly pure bino. (The neutralino can account for most of dark matter when it is mostly a bino.) In this case, $Z_{\chi 1}$ is nearly 1 and the other $Z_{\chi i}$ are very small. Then, the spin dependent term is approximately

$$\begin{aligned}\alpha_{2i} \;\simeq\; & \frac{1}{4(m_{1i}^2 - m_\chi^2)}\left[\left|\eta_{11}^*\frac{y_i}{2}g' Z_{\chi 1}\right|^2 + \left|\eta_{12}^* e_i g' Z_{\chi 1}^*\right|^2\right] \\ & + \frac{1}{4(m_{2i}^2 - m_\chi^2)}\left[\left|\eta_{21}^*\frac{y_i}{2}g' Z_{\chi 1}\right|^2 + \left|\eta_{22}^* e_i g' Z_{\chi 1}^*\right|^2\right]\end{aligned} \tag{20}$$

Hence, in this limit, the spin dependent cross-section will depend on the phases primarily through their effect on the mass of the neutralino, although the magnitude of the η_{ij} will vary significantly, as well, if $R_i|\mu|$ is comparable to $|A_i|$ (see (2)).

To approximate the spin-independent term is somewhat more complicated due to the light scalar Higgs exchange. Keeping the leading terms we find

$$\begin{aligned}
\alpha_{3i} \simeq & -\frac{1}{2(m_{1i}^2 - m_\chi^2)} Re\left[\left(-\eta_{12}^* e_i g' Z_{\chi 1}^*\right)\left(\eta_{11}^* \frac{y_i}{2} g' Z_{\chi 1}\right)^*\right] \\
& - \frac{1}{2(m_{2i}^2 - m_\chi^2)} Re\left[\left(-\eta_{22}^* e_i g' Z_{\chi 1}^*\right)\left(\eta_{21}^* \frac{y_i}{2} g' Z_{\chi 1}\right)^*\right] \\
& + \frac{g g' m_{qi}}{4 m_w m_{H_2}^2 B_i}\left[Re\left(\delta_{1i} Z_{\chi 1}\right) D_i C_i + Re\left(\delta_{2i} Z_{\chi 1}\right) D_i^2\right] \qquad (21)
\end{aligned}$$

Due to the relative size of the Higgs mass to the squark masses, and the smallness of η_{12} to η_{11}, the Higgs exchange term can dominate in α_3. In this limit, the spin-independent cross-section will depend on the phases through the mass of the neutralino, the phases in $Z_{\chi 1}$, and the phases in $Z_{\chi 3,4}$ which exhibit a strong dependence on θ_μ. It would be expected, then, that the spin-independent term should be more sensitive to the changes in the CP phases as we will show below. We have not included the effect of the CP violating phases on the light Higgs mass [20], which will typically be shifted by a few GeV for the masses and phases we study.

4 Results

Using the analytic expressions for the cross-section, we first show a set of contour plots on the $M_2 - \mu$ plane for specific values of A_f, $M_{L(R)}$, $\tan\beta$, and θ_A. In Figures 1 – 6, we display the total cross-section, spin-dependent cross-section, and spin-independent cross-section for both ^{73}Ge (Figs. 1 – 3) and ^{19}F (Figs. 4 – 6). In these plots, the electric dipole moment constraints of the electron, neutron and mercury atom have not been imposed in order to show the general behavior of the cross-section as θ_μ changes. The second set of plots (Figs. 7 – 10) are scatter plots over the MSSM parameter space projected onto the $M_2 - \mu$ plane, concentrating on regions where the electric dipole constraints are satisfied. These plots serve as an existence proof that new CP violating phases can have a significant effect on the scattering rates while still satisfying the EDM constraints. Again, separate scatter plots will be made for ^{73}Ge and ^{19}F.

4.1 General Behavior

In Figs. 1 – 6, we set $A_f = 3000$ GeV, $\tan\beta = 3$, $m_0 = 100$ GeV, $m_A = 300$ GeV and $\theta_A = \pi/2$. A_t is set to its quasi-fixed point value $\simeq 2m_{1/2}$. The value of A_f is chosen for easy comparison with Figures 7–8, where large A_f is necessary to satisfy the electric dipole moments constraints. Figures 1a–c show how the total cross-section for scattering off of ^{73}Ge changes as θ_μ changes from 0 to $\pi/4$. The most significant change occurs in the lower right quadrant. To determine what causes this change, the spin-independent and spin-dependent cross-sections are plotted separately in Figs. 2 and 3. Direct detection experiments typically are sensitive to primarily one or the other type of interaction, and it is important to understand how the phases affect the different cross-sections. In Figs. 2a–c, we see that the spin-dependent cross-section varies only very mildly with θ_μ. In contrast, Figs. 3a–c show that the spin-independent cross-section (which has a maximum near the line $\mu = M_2/2$, where the bino-Higgsino mixing is large) for ^{73}Ge does change significantly, by up to a factor of 2, as θ_μ is varied from 0 to $\pi/4$, and the effect is largest in the lower right quadrant of the plane. The total cross-section's change is due to the large change in the spin-independent cross-section.

Figures 4–6 are the corresponding pictures for ^{19}F. Again, the spin-dependent cross-section does not change much as θ_μ increases, while the spin-independent term undergoes a significant change. Since ^{19}F is so light, the spin-independent term is comparable to the spin-dependent term over much of the parameter space. The total cross-section is affected by the change in θ_μ in those regions where the spin-independent scattering cross-section dominates (for large $|\mu|$ and small M_2) and only little affected in the regions where the spin-dependent scattering cross-section dominates (for large M_2 and small $|\mu|$).

4.2 Behavior with EDM Constraints

When the CP-violating phases are non-zero, the MSSM predicts a non-zero electric dipole moment for the electron, neutron and the mercury atom. In fact, over much of the parameter space, the values chosen in the previous plots will not satisfy the experimental bounds for the electric dipole moments ($< 10^{-25} e$ cm [30] for the neutron) , ($< 4.2 \times 10^{-27} e$ cm [31] for the electron), and ($< 9 \times 10^{-28} e$ cm [32] for the mercury atom).

Within the MSSM, there are several contributions to the electric dipole moment. For the leptons and quarks, electric dipole moments are induced at one loop via exchange of sfermions, charginos, neutralinos, or gluinos (for quarks). For the neutron, there are additional contributions to the electric dipole moment, beyond the contribution by the quark

EDMs, which include a gluonic contribution and a quark color dipole contribution [11, 33, 15]. For a given set of values of the CP-violating phases, there may be significant cancellations between the individual contributions [14, 15, 16]. In general, the electric dipole moment of the electron provides a more stringent constraint over the $M_2 - \mu$ plane than does the neutron electric dipole moment, especially when uncertainties in the computation of d_n are taken into account [34]. It is however, important to have more than one independent experimental constraint on edms, in order to obtain limits on the two CP violating phases. In [34], it was argued that the edm of ^{199}Hg (induced through T-violating nuclear forces [35]) could be used to constrain the MSSM phases. Although it may require some degree of fine tuning, for any given set of $\tan\beta, \mu, M_2, m_0, \theta_{A_i}$, and θ_μ it is always possible to satisfy both of the electric dipole moments by choosing large enough magnitudes for the trilinear mass parameters, A_i [36, 16, 37] (more correctly, acceptable solutions exist for either θ_A or $\theta_A \to \theta_A + \pi$). In the absence of tuning the sfermion masses, the phases must take on values of order $10^{-2} - 10^{-3}$ in order to satisfy the EDM constraints.

For figures 7 – 10, a general scan of parameter space was performed over the M_2, μ, A, and m_0 while setting A_t again equal to the quasi-fixed point. We have again taken $\tan\beta = 3$ and $m_A = 300$ GeV. The range of parameters is chosen via several criteria. From LEP2's search for charginos, there is a lower bound on the mass of the chargino of 95 GeV [38]. This implies a restriction on the lower values of M_2 and μ of around 100 GeV. We also insist that the neutralino be the LSP, and we employ the recent LEP2 constraint on sfermion masses and discard runs with $m_{\tilde{t}} < 80$ GeV [38]. Furthermore, when the sfermions are very massive and the LSP is gaugino-like, the neutralino's relic density is too large to be compatible with the observational lower limits on the lifetime of the universe [39]. Therefore for simplicity, we restrict the values of m_0 so as to give cosmologically reasonable relic densities for all neutralino compositions (although of course m_0 is not constrained for Higgsino-like LSP's).

In each figure, θ_A and θ_μ are fixed, and a scan is performed over $M_2, |\mu|, A$, and m_0. If a set of parameters satisfies the EDM constraints, the value of the cross-section is calculated and compared to the value of the cross-section when θ_A and θ_μ are both zero. This scan is then projected onto the $M_2 - \mu$ plane. Figs. 7a and 7b are for ^{73}Ge for $\theta_\mu = \pi/8, \theta_A = 3\pi/8$ and $\theta_\mu = \pi/4, \theta_A = \pi/2$, respectively, and 8a and 8b are the corresponding figures for ^{19}F. In Figures 7 and 8, we require both the electron and neutron edm limits to be satisfied. For Figs. 7a and 8a, the range of parameters is: 200 GeV $\leq M_2 \leq$ 800 GeV, 100 GeV $\leq \mu \leq$ 1000 GeV, 100 GeV $\leq m_0 \leq$ 200 GeV, and 2200 GeV $\leq A \leq$ 3500 GeV. In the scan, M_2 is incremented every 20 GeV, μ every 20 GeV, m_0 every 25 GeV, and A every 25 GeV. For figures 7b and 8b, the range of parameters is: 150 GeV $\leq M_2 \leq$ 400 GeV, 100 GeV $\leq \mu \leq$

1000 GeV, 100 GeV $\leq m_0 \leq$ 200 GeV, and 2700 GeV $\leq A \leq$ 3500 GeV. In the scan, M_2 was incremented every 10 GeV, μ every 20 GeV, m_0 every 10 GeV, and A every 25 GeV. We bin the resulting $\sigma(\theta_\mu, \theta_A \neq 0)/\sigma(\theta_\mu, \theta_A = 0)$ in steps of 0.1. A single symbol at a point means that every parameter set satisfying the EDM constraints has a cross-section ratio in the specified range. Some grid points have two symbols. Notice for all of the diagrams, there are regions where the cross-section is reduced. For some of the diagrams, however, there are regions where the cross-section is enhanced. In figures 7b and 8b, when $\theta_\mu = \pi/4$ and $\theta_A = \pi/2$ there are regions where the cross-section decreases by up to a factor of 2. Although this region of parameter space is small (in the region of 200 GeV$\leq M_2 \leq$ 300 GeV and μ around 750 GeV), it has cosmological significance because it is in a region of parameter space where the neutralino is most nearly a bino, so that the neutralino can account for most of dark matter. By comparing the scatterplots to the previous contour plots, the largest changes identified by the scatterplots correspond to the region of parameter space that has the smallest cross-section for both ^{73}Ge and ^{19}F.

In [5], we had found cases in which the cross-section was reduced by over an order of magnitude for certain values of the phases. Those results show the maximum possible effect and such a reduction occurs at a different value of θ_μ for each choice of M_2 and μ. Here, we have a milder effect, but one that should be taken as relatively generic. We have chosen two specific values of θ_μ, and scan the M_2-μ plane. Therefore, in most cases, we will miss the value of θ_μ for which the cancellation in the cross-section is at a maximum. Furthermore, we have lost a considerable amount of parameter space due to the imposition of the EDM constraints. This space could be enlarged if we were to relax the universality on the A-terms. By adjusting A_e and A_q separately, a larger portion of the plane would survive and larger effects would be visible.

In Figures 9 and 10, we show the results when both the electron and mercury edms are satisfied. Figures 9a and 10a use the same range of parameters as those in figures 7a and 8a. Likewise, figures 9b and 10b use the same parameters as those in figures 7b and 8b. The variation of the cross-section in these plots is very similar to the variation of the cross-section when the neutron and electron edms are imposed (figures 7 and 8) but a different section of the $M_2 - |\mu|$ plane is selected. These results (in figures 7 – 10) are in qualitative agreement with those of [6].

It is important to note that we have chosen the ranges for our scans of A to coincide with the regions where cancellations are known to make the electric dipole moments small. As such, each point in Figs.7 – 10a represents about 60 points in the scan (deprojected), and thus we find solutions for about 12% of the total of ∼400,000 points in our scan. Similarly,

each point in Figs.7 – 10b represents only about 10 points in the scan. In this case, we find solutions for about 1% of a total of ∼400,000 points in the scan. These points serve to demonstrate the size of the uncertainties in the elastic scattering rates due to large CP violating phases. Again, the cosmological constraints may be satisfied by taking the first two sfermion generations heavy, while having a light third generation[13]. Lastly, we also note that there are regions at large $m_0(> 1\text{TeV})$ where the phases can be large without any tuning of the mass parameters. However, such large sfermion masses are cosmologically forbidden unless the LSP is mixed or Higgsino-like, in which case there tends to be an insufficient relic LSP abundance to make direct detection relevant.

5 Summary

We have made a comprehensive study of the effect of the two CP violating phases in the MSSM on the neutralino elastic scattering cross-section. Starting with the full 4-Fermi interaction lagrangian between neutralinos and quarks, we examined in detail the effect of the phases of the two dominant terms corresponding to the spin-dependent (α_2) and spin-independent (α_3) parts of the cross-section in the non-relativistic limit.

We have shown explicitly the variation of the cross-section in the M_2-μ plane for neutralino scattering off two sample nuclei, ^{73}Ge and ^{19}F. We showed the extent of the variation for the total cross-section as well as the individual spin-dependent and -independent contributions. It is the spin-independent piece in the bino-portion of the parameter plane that is most sensitive to the CP-violating phases.

We have also considered in detail the regions of the parameter plane which are consistent with the experimental limits on the electric dipole moments of the electron, neutron, and mercury atom. The edms provide a very strong constraint and therefore, some degree of tuning is necessary to satisfy these constraints along with other cosmological and phenomenological constraints as well. In the surviving regions, the cross-section is typically reduced, by as much as a factor of ~ 2.5, while some regions in the M_2-μ plane show slight enhancements in the cross-section by about 10%.

It is also worth mentioning that the relic density of neutralinos is determined by their annihilation rate and the annihilation rate will also depend on the CP violating phases. In the general MSSM, these effect could be large [12] as the typical p-wave suppression of the annihilation cross-section is removed when the left and right handed sfermion masses are nearly degenerate. In the models such as the constrained MSSM (when universal soft masses at the GUT scale are assumed) this effect is small [14]. There is however, another contribution to

the annihilation cross-section which is unique to the presence of non-vanishing CP-violating phases. In the effective Lagrangian (3), terms which go as $\bar{\chi}\gamma^5\chi$ will be proportional to the three momentum of the neutralinos and will thus be negligible in the non-relativistic limit. However, the term proportional to α_{5i} will give non-negligible contributions to the annihilation rate for non-zero CP violating phases as can be seen by examination of eq.(8). In the non-relativistic limit we have

$$\sigma v_{rel} = \sum_f \frac{2}{\pi} \left|\alpha_{5i}\right|^2 m_\chi^2 \left(1 - \frac{m_f^2}{m_\chi^2}\right)^{\frac{3}{2}} \tag{22}$$

where the total contribution should be summed over all fermions, f, which are less massive then the neutralino. Note that in the limit of vanishing CP violating phases, α_{5i} is zero since it depends on the imaginary contribution to (10). A complete investigation of the effects of the phases on the total annihilation cross-section is left for future study.

Acknowledgments

The work of K.O. was supported in part by DOE grant DE–FG02–94ER–40823. The work of T.F. was supported in part by DOE grant DE–FG02–95ER–40896 and in part by the University of Wisconsin Research Committee with funds granted by the Wisconsin Alumni Research Foundation.

References

[1] H.E. Haber and G.L. Kane, Phys. Rep. **117** (1985) 75.

[2] J. Ellis, J.S. Hagelin, D.V. Nanopoulos, K.A. Olive and M. Srednicki, Nucl. Phys. **B238** (1984) 453.

[3] See, e.g., David O. Caldwell, in Proceedings of the Fifth International Workshop on Topics in Astroparticle and Underground Physics, 1997.

[4] G. Jungman, M. Kamionkowski, and K. Griest, *Phys. Rep.***267**, 195 (1996).

[5] T. Falk, A. Ferstl, and K.A. Olive, Phys. Rev. **D59** (1999) 055009.

[6] U. Chattopadhyay, T. Ibrahim, and P. Nath, hep-ph/9811362.

[7] S. Khalil and Q. Shafi, hep-ph/9904448.

[8] M. Dugan, B. Grinstein and L. Hall, Nucl. Phys. **B255**, 413 (1985).

[9] J. Ellis, S. Ferrara, and D. V. Nanopoulos, *Phys. Lett.* B**114** (1982) 231; W. Buchmüller and D. Wyler, *Phys. Lett.* B**121** (1983) 321; J. Polchinski and M. Wise, *Phys. Lett.* B**125** (1983) 393; F. del Aguila, M. Gavela, J. Grifols, and A. Mendez, *Phys. Lett.* B**126** (1983) 71; C. V. Nanopoulos and M. Srednicki, *Phys. Lett.* B **128** (1983) 61.

[10] P. Nath, Phys. Rev. Lett. **66** (1991), 2565.

[11] Y. Kizukuri and N. Oshimo, *Phys. Rev.* D**45** (1992) 1806; *Phys. Rev.* D**46** (1992) 3025.

[12] T. Falk, K.A. Olive, M. Srednicki *Phys. Lett.* B**354**, 99 (1995).

[13] S. Dimopoulos and G.F. Giudice, Phys. Lett. **B357** (1995) 573 ; A. Cohen, D.B. Kaplan and A.E. Nelson, Phys. Lett. **B388** (1996) 599 ; A. Pomarol and D. Tommasini, Nucl. Phys. **B488** (1996) 3.

[14] T. Falk and K.A. Olive, Phys. Lett. **B375** (1996) 196.

[15] T. Ibrahim, P. Nath, *Phys. Rev.* D**57** (1998) 478; Erratum *Phys. Rev.* D**58**, 019901 (1998); T. Ibrahim, P. Nath, *Phys. Lett.* B**418** (1998) 98; T. Ibrahim, P. Nath, *Phys. Rev.* D**58** (1998) 111301.

[16] T. Falk and K.A. Olive, Phys. Lett. **B439** (1998) 71.

[17] T. Ibrahim and P. Nath, Phys. Rev. **D58** (1998) 111301; M. Brhlik, G. J. Good and G.L. Kane, Phys. Rev. **D59** (1999) 115004.

[18] S. Pokorski, J. Rosiek, and C.A. Savoy, hep-ph/9906206.

[19] A. Pilaftsis, Phys. Rev. D **58** (1998) 096010; A. Pilaftsis, Phys. Lett. **435B** (1998) 88; D. A. Demir, hep-ph/9901389; D. A. Demir, hep-ph/9905571.

[20] A. Pilaftsis and C.E.M. Wagner, hep-ph/9902371.

[21] M. Carena, M. Olechowski, S. Pokorski, and C. E. M. Wagner, *Nucl. Phys.* B**426**, 269 (1994).

[22] J. Ellis and R. Flores, *Phys. Lett.* B**300**, 175 (1993).

[23] H. Cheng, *Phys. Lett.* B**219**, 347 (1989).

[24] J. Ellis and R. Flores, *Nucl. Phys.* B**307**, 883 (1988).

[25] K. Griest *Phys. Rev.* D**38**, 2357 (1988).

[26] The Spin Muon Collaboration, D. Adams *et. al.*, *Phys. Lett.* B**329**, 399 (1994).

[27] M. A. Shifman, A. I. Vainshtein, and V. I. Zakharov, *Phys. Lett.* **78B**, 443 (1978); A. I. Vainshtein, V. I. Zakharov, M. A. Shifman, *Usp. Fiz. Nauk* **130**, 537 (1980).

[28] J. Gasser, H. Leutwyler, and M. E. Sainio, *Phys. Lett.* B**253**, 252 (1991).

[29] M. Drees and M. M. Nojiri, *Phys. Rev.* D**47**, 4226 (1993); M. Drees and M. M. Nojiri, *Phys. Rev.* D**48**, 3483 (1993).

[30] I. S. Altarev *et al.*, Phys. Lett **B276** (1992) 242.

[31] E. Commins *et al.*, Phys. Rev. **A50** (1994) 2960.

[32] J.P. Jacobs *et al.*, Phys. Rev. Lett. **71** (1993) 3782; J.P. Jacobs *et al.*, Phys. Rev. **A52** (1995) 3521.

[33] S. Weinberg, Phys. Rev. Lett. **63** (1989) 2333; R. Arnowitt, M. Duff, and K. Stelle, Phys. Rev. **D43** (1991) 3085.

[34] T. Falk, K.A. Olive, M. Pospelov, and R. Roiban, hep-ph/9904393.

[35] V.M. Khatsimovsky, I.B. Khriplovich and A.R. Zhitnitsky, Z. Phys. **C36** (1987) 455; V.M. Khatsimovsky, I.B. Khriplovich and A.S. Yelkhovsky, Ann. Phys. **186** (1988) 1; V.M. Khatsimovsky and I.B. Khriplovich, Phys. Lett. **B296** (1994) 219.

[36] R. Garisto and J. Wells *Phys. Rev.* D**55**, 1611 (1997).

[37] E. Accomando, R. Arnowitt and B. Dutta, hep-ph/9907446.

[38] Official compilations of LEP limits on supersymmetric particles are available from: `http://www.cern.ch/LEPSUSY/`

[39] J. Ellis, T. Falk, K.A. Olive and M. Schmitt, Phys. Lett. **B413** (1997) 355; J. Ellis, T. Falk, G. Ganis, K.A. Olive, M. Schmitt, *Phys. Rev.* D**58** (1998) 095002; J. Ellis, T. Falk, and K.A. Olive, Phys. Lett. **B444** (1998) 367; J. Ellis, T. Falk, K.A. Olive, and M. Srednicki, hep-ph/9905481.

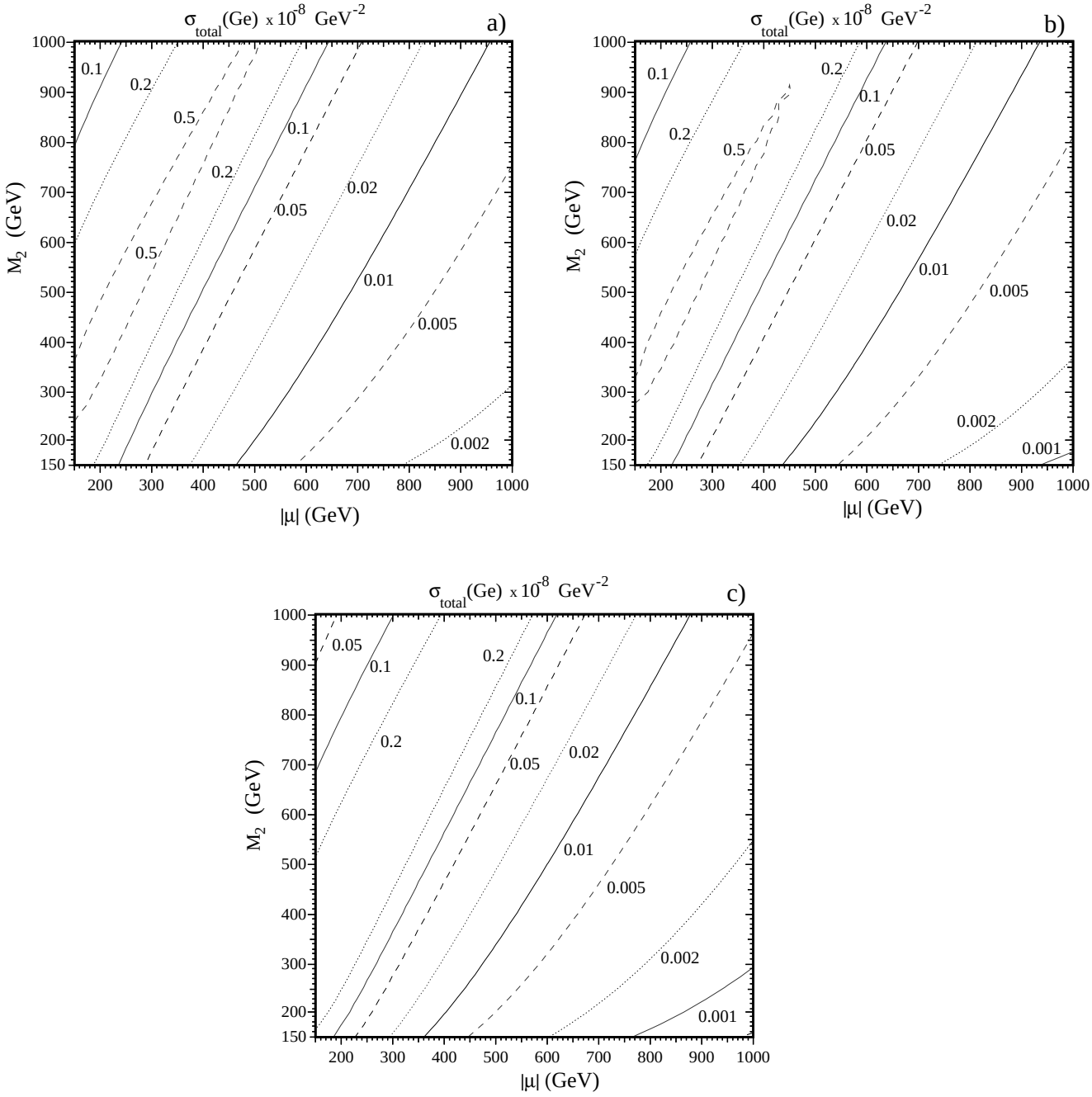

Figure 1: *The total cross-section for elastic scattering off of* ^{73}Ge *a.) for* $\theta_\mu = 0$*, b)* $\theta_\mu = \pi/8$*, c.)* $\theta_\mu = \pi/4$*. All plots have* $\theta_A = \pi/2$*. The axis are in units of GeV. The contours are in units of* 10^{-8} GeV^{-2}*.*

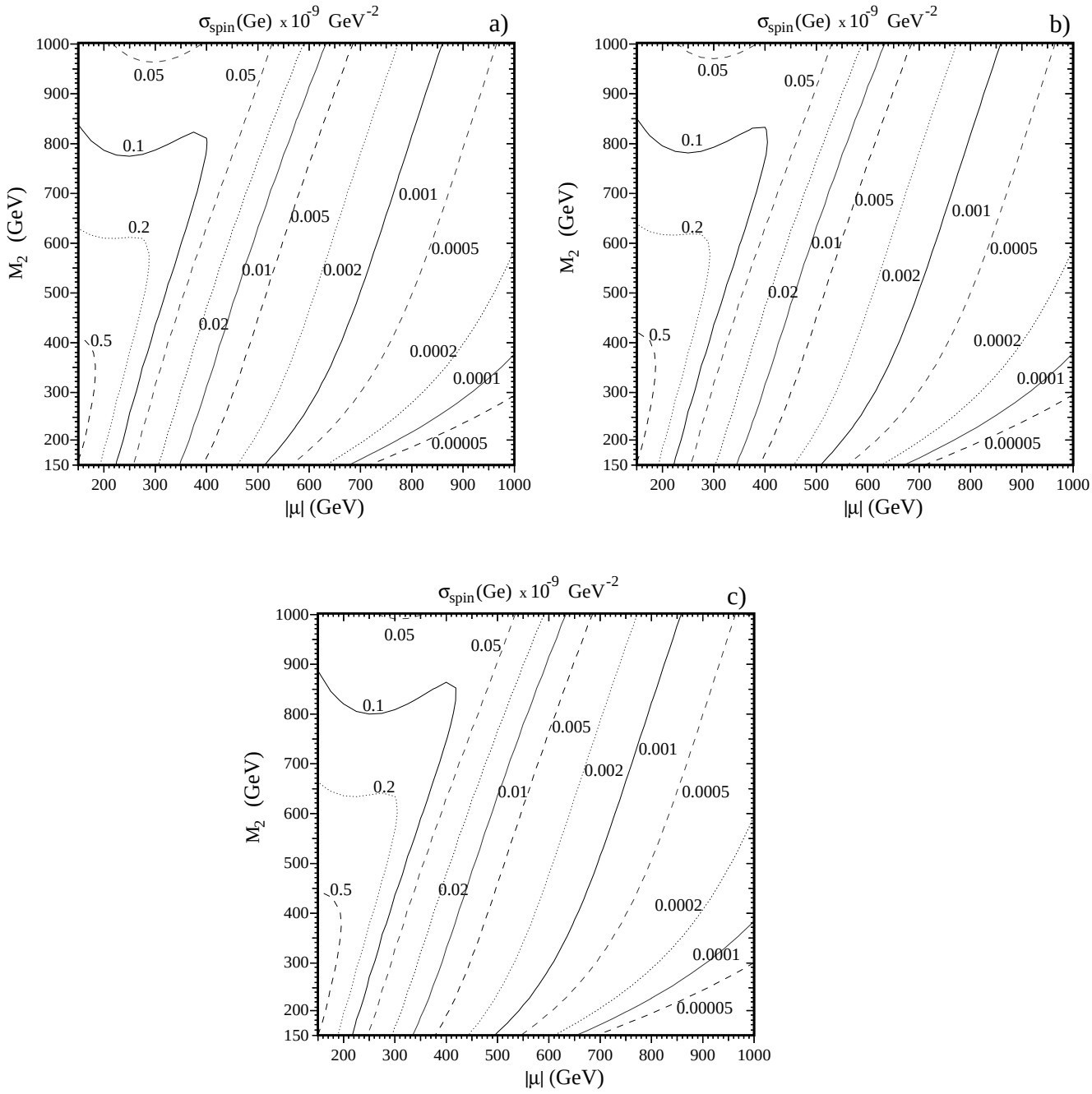

Figure 2: *The spin-dependent cross-section for elastic scattering off of* ^{73}Ge*, for the same parameters as in Fig. 1. The contours are in units of* 10^{-9} GeV^{-2}.

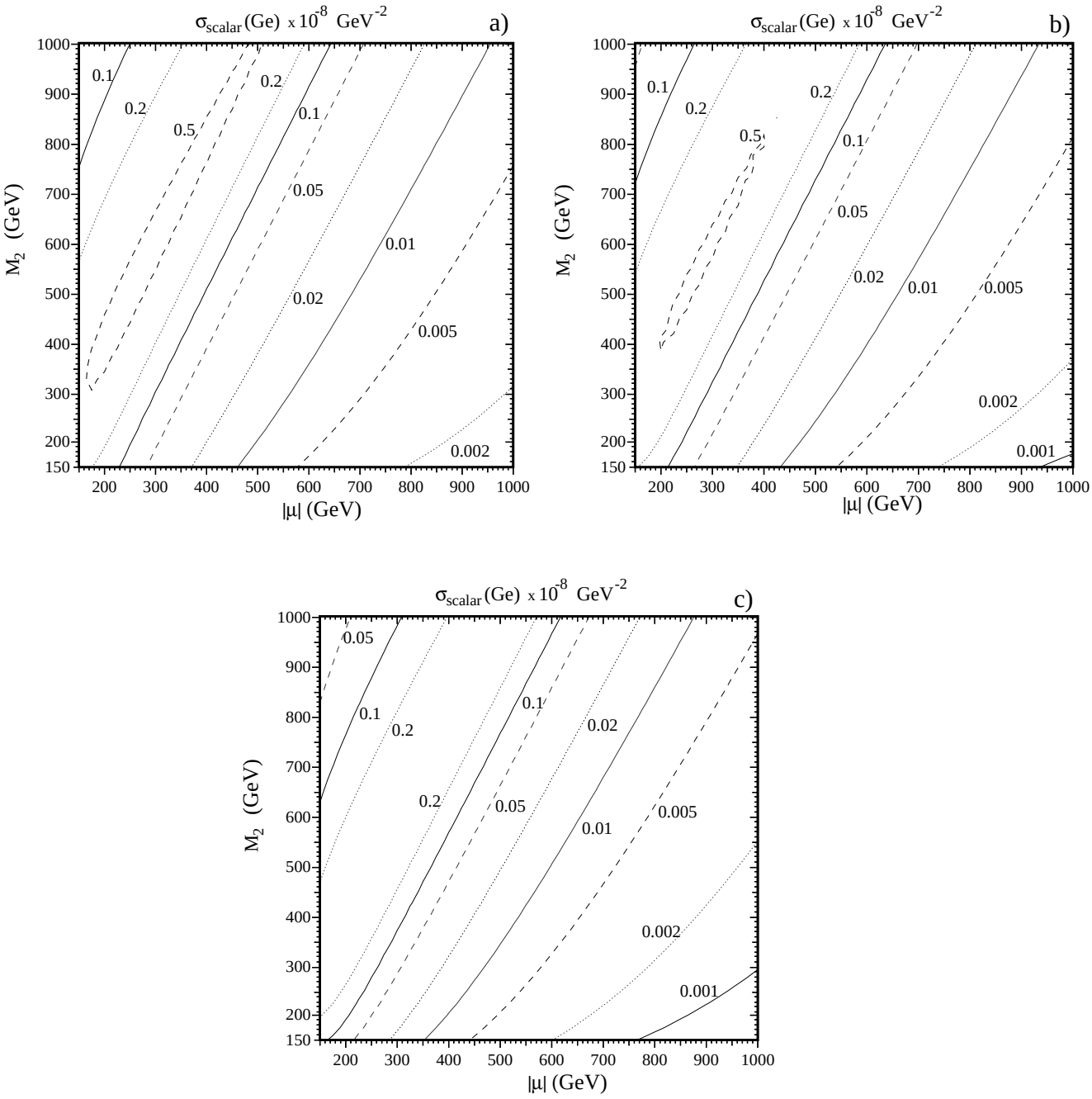

Figure 3: *The spin-independent cross-section for elastic scattering off of* ^{73}Ge*, for the same parameters as in Fig. 1. The contours are in units of* 10^{-8} GeV^{-2}

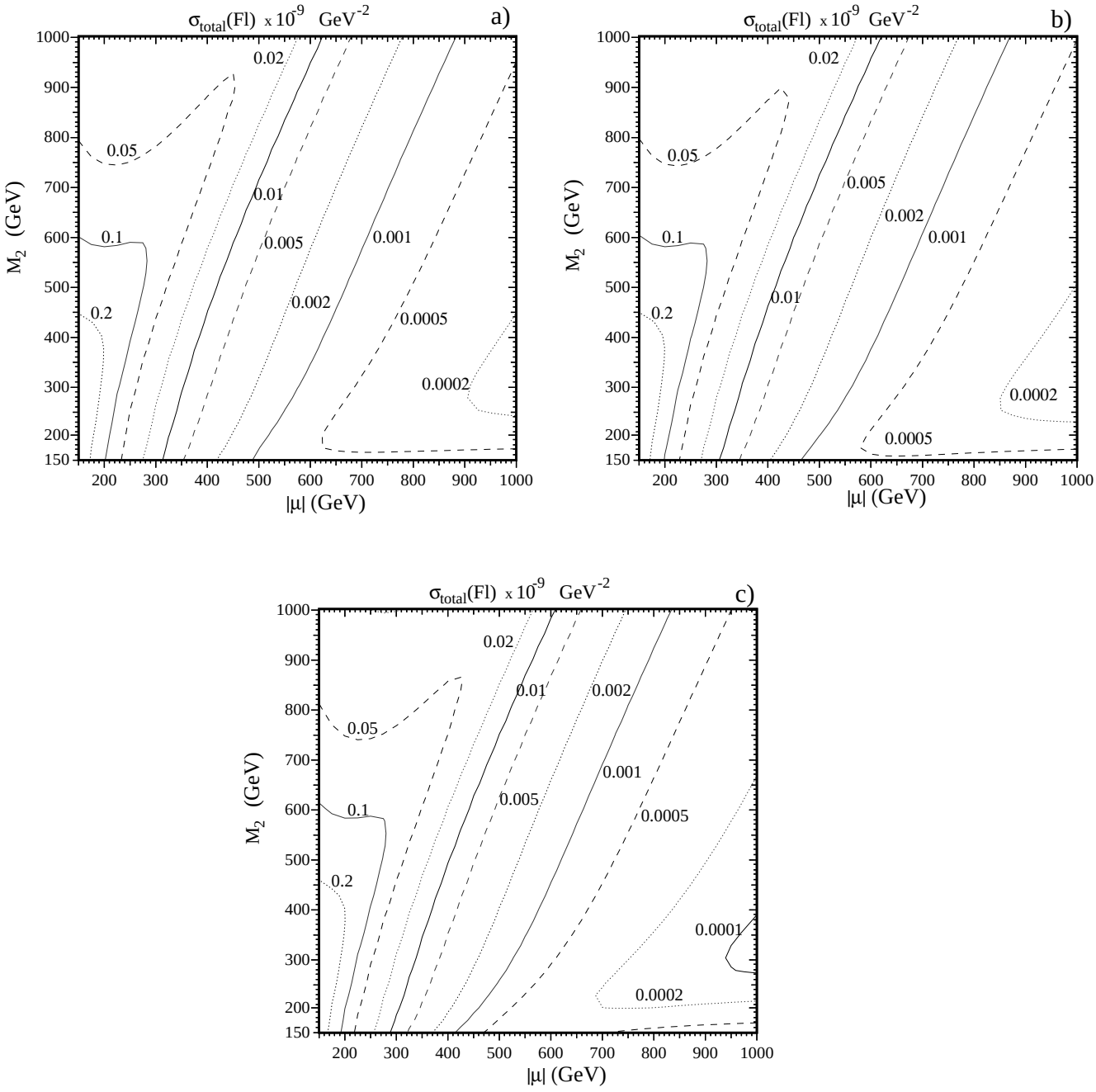

Figure 4: *The total cross-section for elastic scattering off of* ^{19}F *a.) for* $\theta_\mu = 0$*, b)* $\theta_\mu = \pi/8$*, c.)* $\theta_\mu = \pi/4$*. All plots have* $\theta_A = \pi/2$*. The axis are in units of GeV. The contours are in units of* 10^{-9} GeV^{-2}*.*

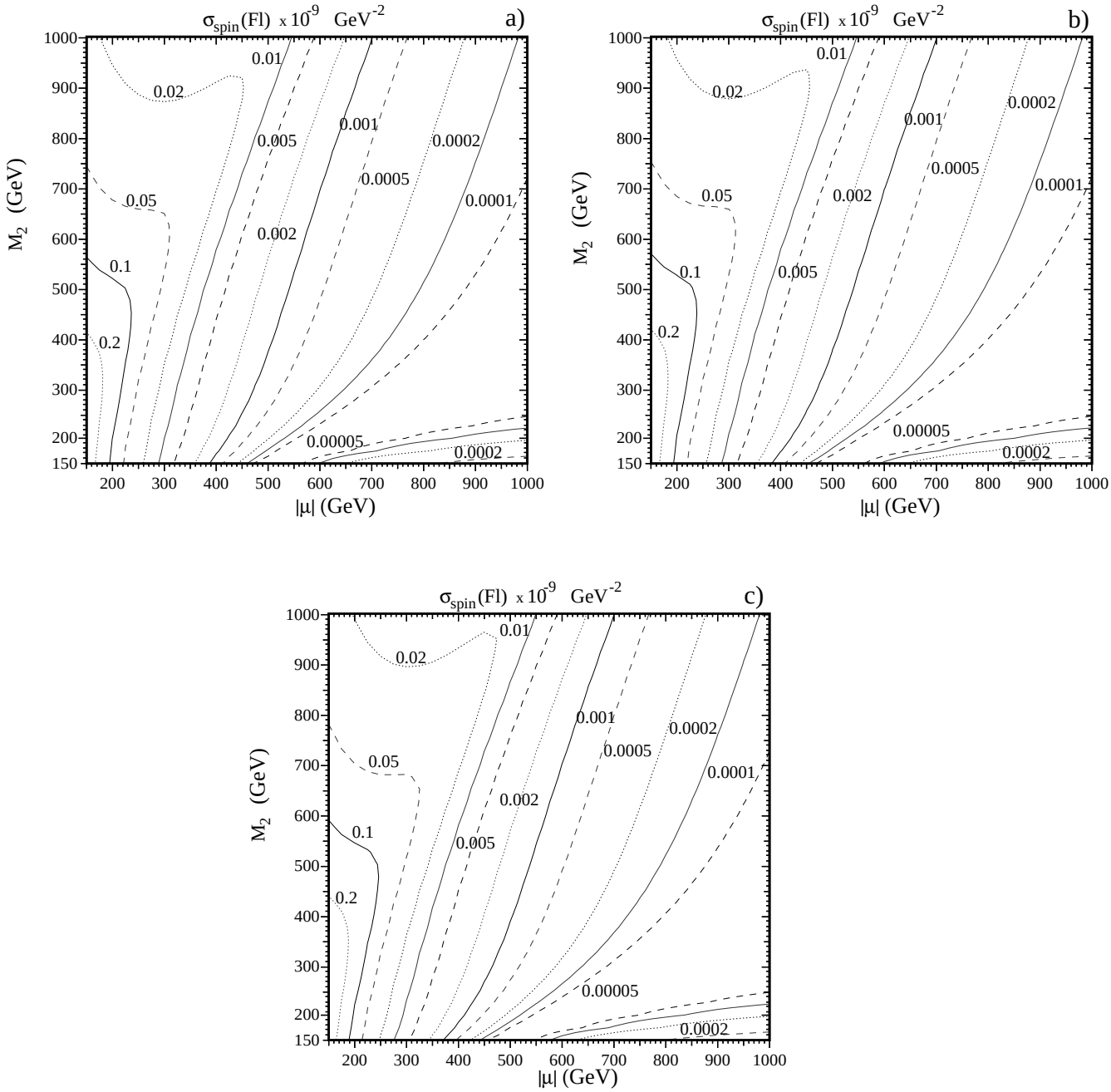

Figure 5: *The spin-dependent cross-section for elastic scattering off of* ^{19}F*, for the same parameters as in Fig. 4. The contours are in units of* 10^{-9} GeV^{-2}.

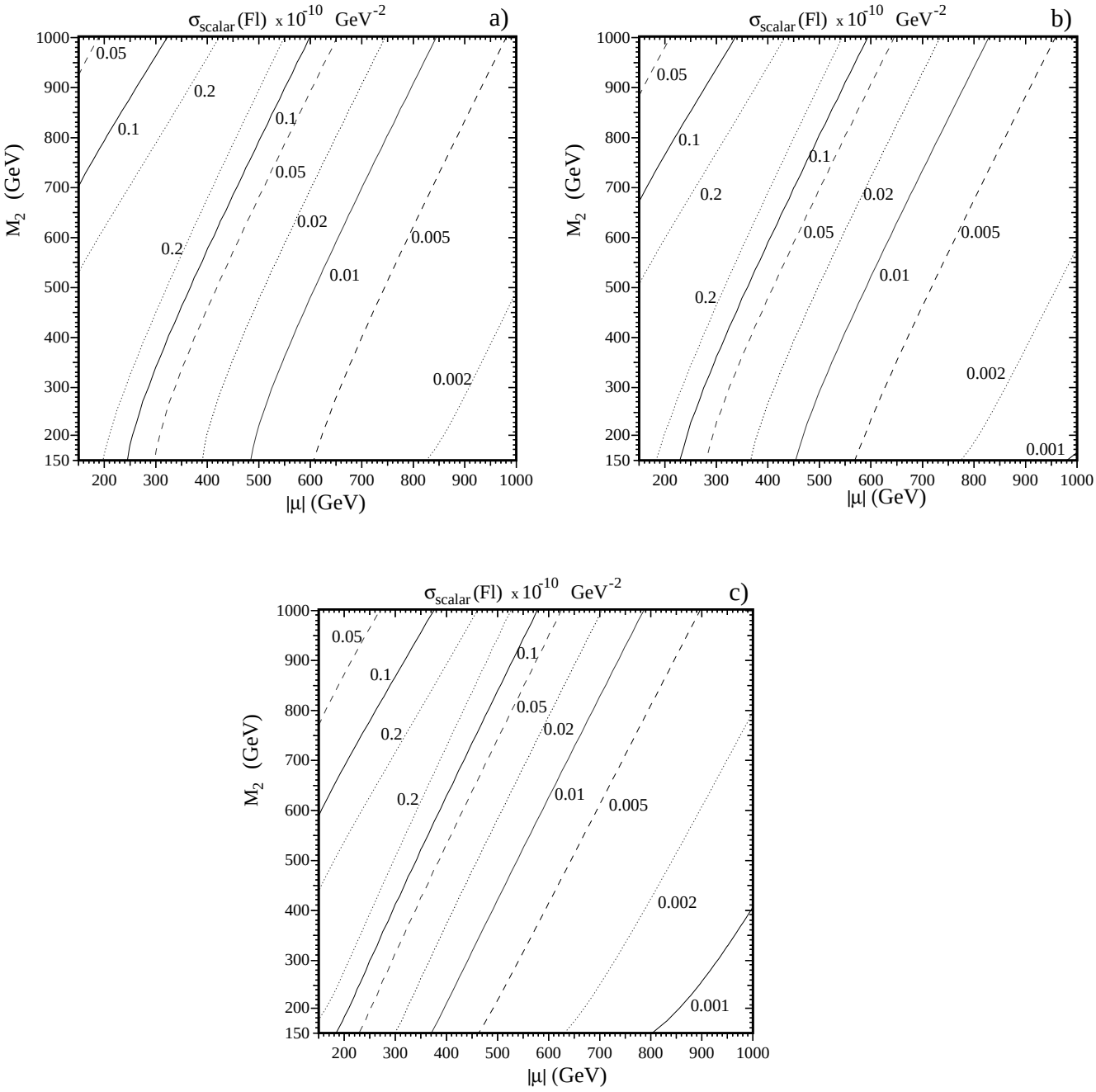

Figure 6: *The spin-independent cross-section for elastic scattering off of* ^{19}F*, for the same parameters as in Fig. 4. The contours are in units of* 10^{-10} *GeV*$^{-2}$.

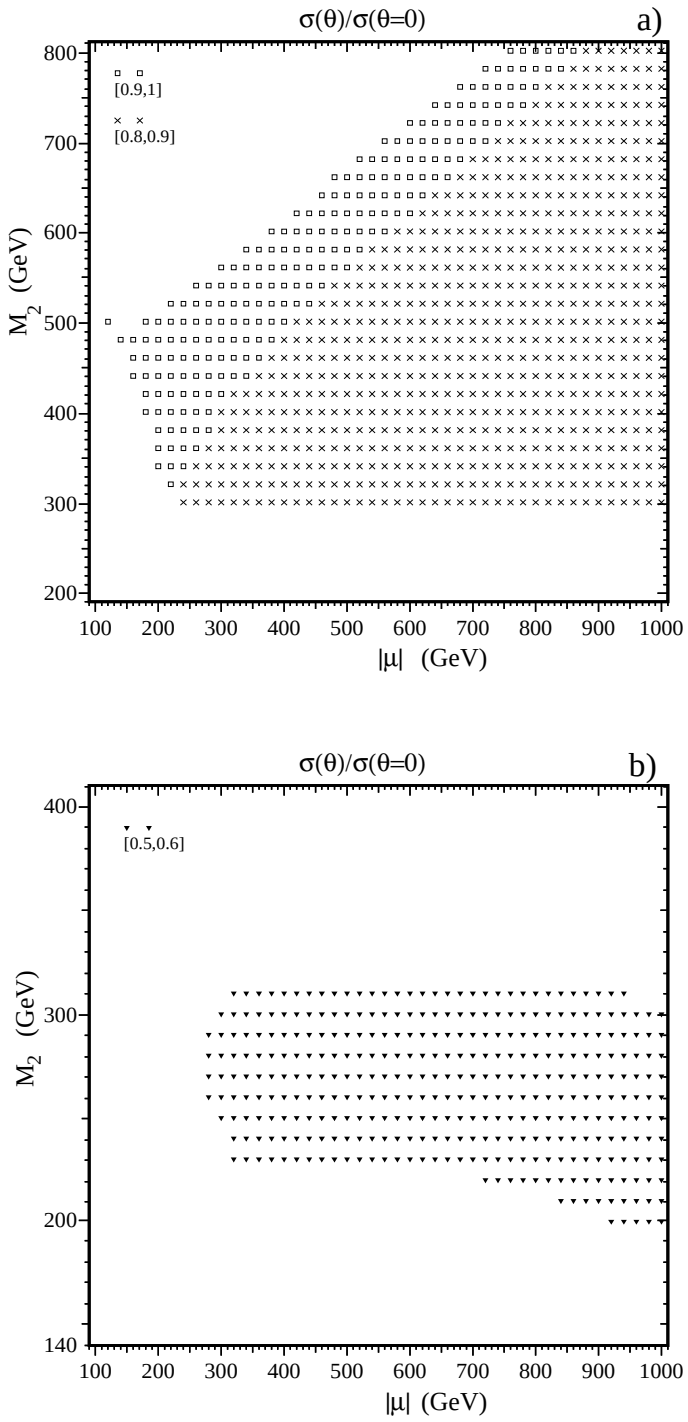

Figure 7: *The ratio of the elastic scattering cross-section with non-vanishing CP violating phases to the cross-section when the CP violating phases are zero, for* ^{73}Ge*. Here, the constraints from the eEDM and nEDM are taken into account and the scan of the parameter space described in the text is projected onto the* $M_2 - \mu$ *plane. In a)* $\theta_\mu = \pi/8, \theta_A = 3\pi/8$ *and b)* $\theta_\mu = \pi/4$*,* $\theta_A = \pi/2$*.*

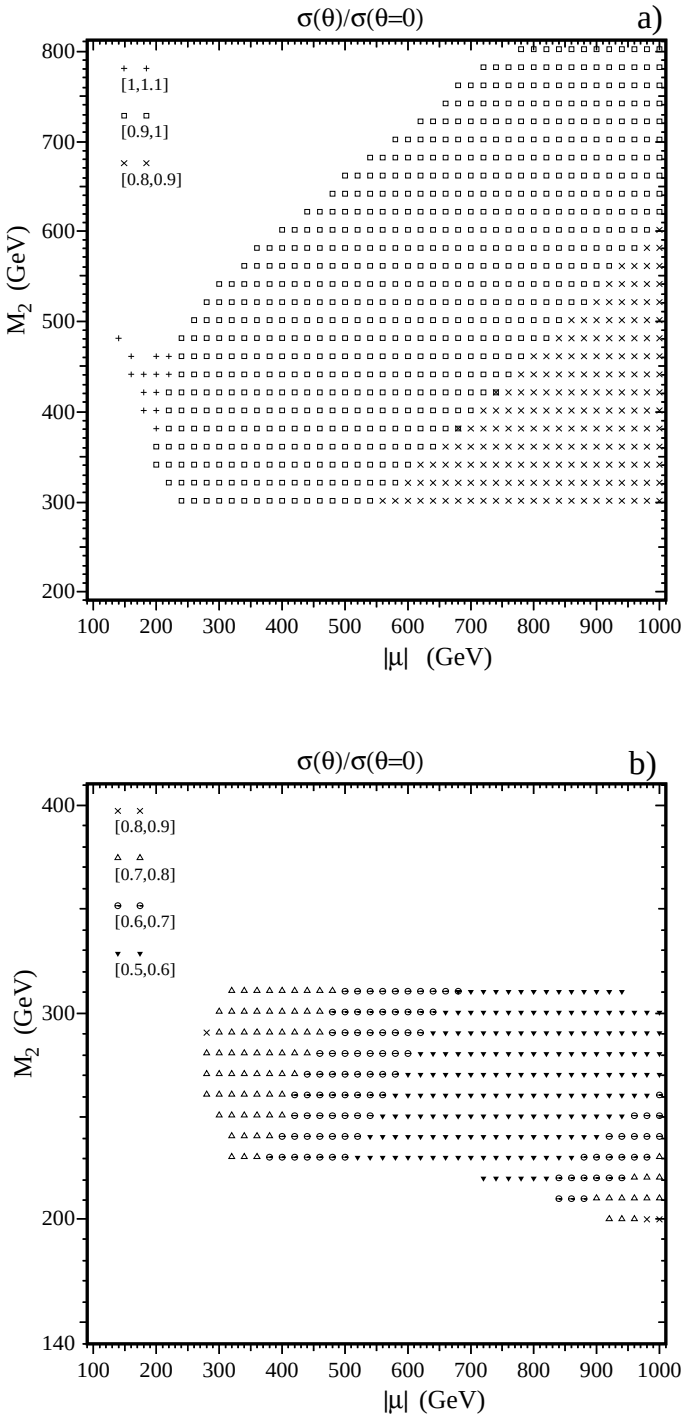

Figure 8: *Same as Fig. 7 for* ^{19}F.

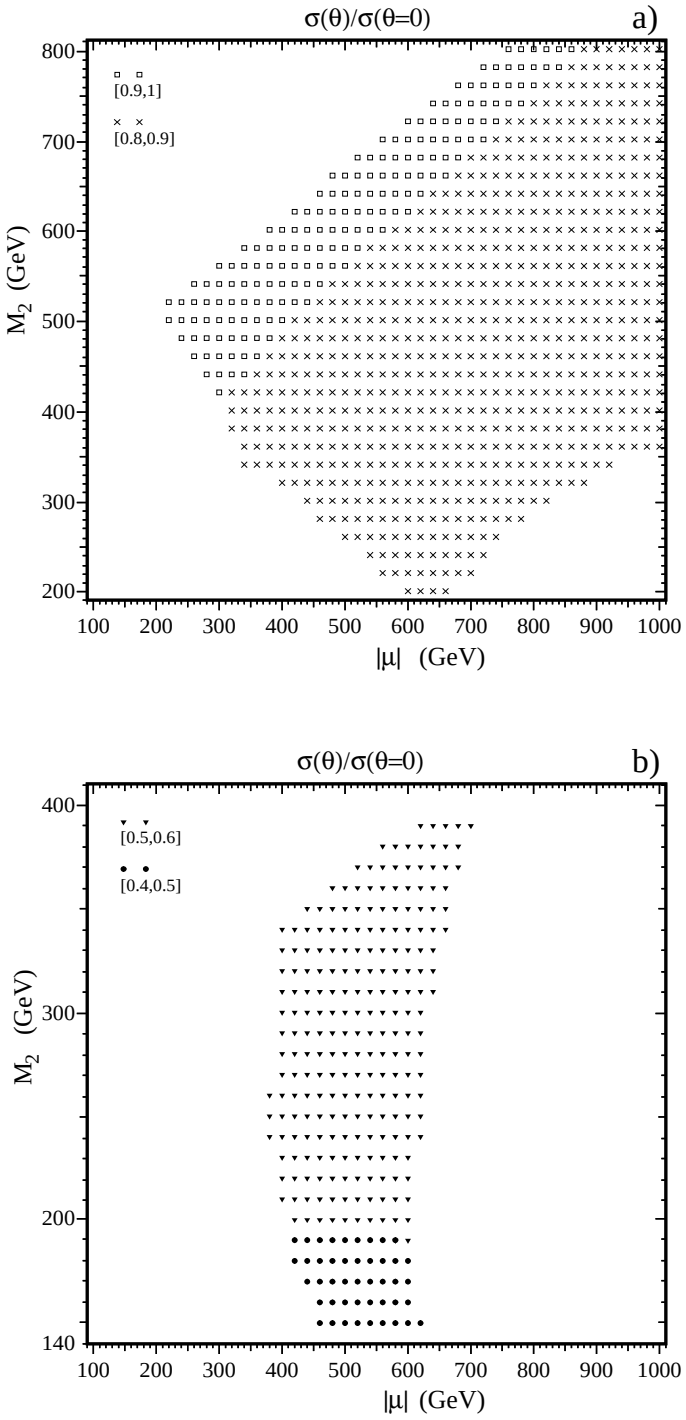

Figure 9: *Same as Fig. 7 using the constraints from the eEDM and the HgEDM.*

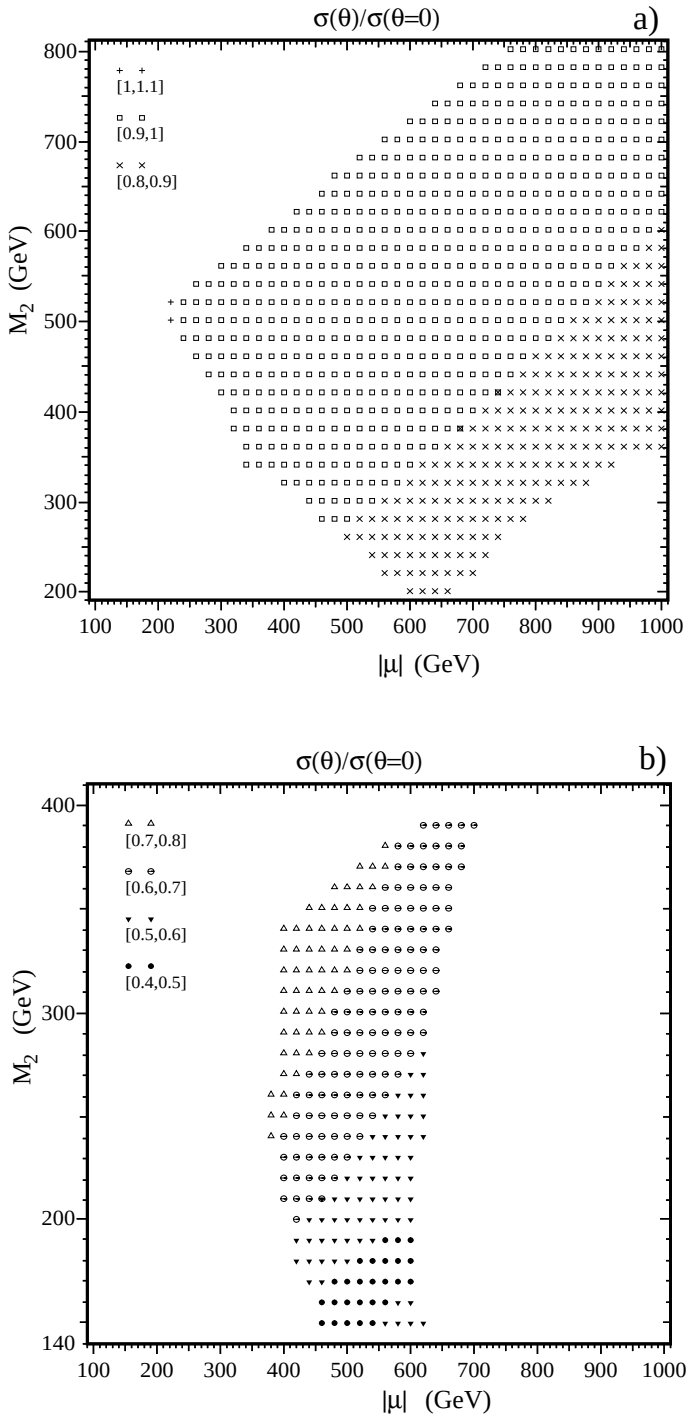

Figure 10: *Same as Fig. 9 for* ^{19}F.